A complete coverage of log-cumulant space in terms of distributions for Polarimetric SAR data

Lionel Bombrun, Stian Normann Anfinsen, Olivier Harant

A COMPLETE COVERAGE OF LOG-CUMULANT SPACE IN TERMS OF DISTRIBUTIONS FOR POLARIMETRIC SAR DATA

Lionel Bombrun[1], **Stian Normann Anfinsen**[2], **and Olivier Harant**[3,4]

[1]*Université de Bordeaux, UB1, IPB, ENSEIRB-Matmeca, Laboratoire IMS, UMR 5218, Groupe Signal et Image, Talence, France, lionel.bombrun@ims-bordeaux.fr*

[2]*University of Tromsø, Department of Physics and Technology, NO-9037 Tromsø, Norway, stian.normann.anfinsen@uit.no*

[3]*Grenoble Image Parole Signal et Automatique (GIPSA-lab), CNRS INPG, Saint-Martin-d'Hères, France, olivier.harant@gipsa-lab.grenoble-inp.fr*

[4]*IETR Laboratory, SAPHIR Team, University of Rennes 1, Rennes, France*

ABSTRACT

In this paper, we introduce two new families of probability density functions (PDFs) for the polarimetric target vector and covariance matrix. These families complete the diagram spanned by the second and third-order matrix log-cumulants of the data, and contribute to a holistic theory for statistical modeling of Polarimetric Synthetic Aperture Radar (PolSAR) data based on the Spherically Invariant Random Vector (SIRV) model. The new PDFs result from using a Beta and an Inverse Beta distributed texture variable, and are referred to as the $\mathcal{W}$ and $\mathcal{M}$ distributions. They are able to model data with low variance but extreme skewness, which proves particularly relevant for speckle filtered data with textural variability. The usefulness of the models is demonstrated with multi-frequency real data.

Key words: Polarimetric SAR, Matrix log-cumulant diagram, Texture modeling.

1. INTRODUCTION

For low resolution Polarimetric SAR (PolSAR) images, it is generally sufficient to model the variability of distributed targets as fully developed speckle. This assumption leads to the complex multivariate Gaussian distribution for single-look data and the complex Wishart distribution for multilook data, that have been widely used in many application such as filtering, classification (1) and change detection. With the new high resolution PolSAR sensors, the number of scatterers present in each resolution cell decreases considerably, which renders the former assumption invalid. To account for this, alternative clutter models have been proposed in the literature founded on the product model. In this model, the spatial heterogeneity of the mean radar reflectivity is incorporated by introducing a scalar random variable τ representing the natural variability of the target, referred to as texture. For single-look data, the observed target vector $\mathbf{k}$ is decomposed as the product between the square root of τ and an independent, zero mean, complex, circular Gaussian random vector $\mathbf{z}$, representing fully developed speckle. For multilook data, the observed covariance matrix $[T]$ is expressed as the product of $\tau[M]$, where the covariance matrix $[M]$ follows a complex Wishart distribution.

For the texture modeling of PolSAR data, distributions from the Pearson system are commonly used. This system consists of a set of distributions families, including the Gaussian, Gamma and Beta ones. In this paper, the authors derive the analytical expressions of the target vector (for single-look data) and covariance matrix (for multilook data) PDFs for Gamma, Inverse Gamma, Fisher, Beta and Inverse Beta distributed texture. They are respectively the $\mathcal{K}$ (2), $\mathcal{G}^0$ (3), KummerU (4), $\mathcal{W}$ and $\mathcal{M}$ distributions. The benefit of these multivariate distributions will be shown by plotting the texture log-cumulant diagram (5) for different frequency bands (C-, L- and P-bands) over the Nezer forest.

This paper is organized as follows. In Section 2, the context of PolSAR clutter modeling and the matrix log-cumulant diagram are first introduced. Then, in Section 3, an overview of the multivariate PolSAR models for both single-look and multi-look is drawn. The utility of those models is demonstrated with multi-frequency real data in Section 4. Finally, some conclusion and perspectives of this work are discussed in Section 5.

2. POLSAR CLUTTER MODELING

2.1. SIRV model

In the PolSAR context, the target vector $\mathbf{k}$ is a complex vector of length p ($p = 3$ if the reciprocity assumption

holds), and could be written under the SIRV model hypothesis as the product of a square root of a positive random variable τ (representing the texture) with an independent circular complex Gaussian vector $\mathbf{z}$ with zero mean and covariance matrix $[M] = E\{\mathbf{z}\mathbf{z}^H\}$ (representing the speckle):

$$\mathbf{k} = \sqrt{\tau}\,\mathbf{z}, \tag{1}$$

where the superscript H denotes the complex conjugate transposition and $E\{\cdot\}$ the mathematical expectation.

The SIRV representation is not unique, so a normalization condition is necessary. Classically, the normalization is imposed on the trace of the covariance matrix, chosen here to p the dimension of target scattering vector. For a given covariance matrix $[M]$, the ML estimator of the texture for the pixel i (τ_i) is given by:

$$\hat{\tau}_i = \frac{\mathbf{k}_i^H [M]^{-1} \mathbf{k}_i}{p}. \tag{2}$$

The ML estimator of the normalized covariance matrix under the deterministic texture case is the solution of the following recursive equation :

$$[\hat{M}]_{FP} = f([\hat{M}]_{FP}) = \frac{p}{N} \sum_{i=1}^{N} \frac{\mathbf{k}_i \mathbf{k}_i^H}{\mathbf{k}_i^H [\hat{M}]_{FP}^{-1} \mathbf{k}_i}, \quad \text{with} \quad \mathrm{tr}([\hat{M}]_{FP}) = p. \tag{3}$$

The existence and the uniqueness, up to a scalar factor, of the Fixed Point estimator of the normalized covariance matrix, as well as the convergence of the recursive algorithm whatever the initialization have been established (6).

Practically, the covariance matrix is first estimated according to (3), then the N texture random variables $(\tau_1, \ldots, \tau_N)$ are derived by (2). When the texture is assumed to be deterministic, the ML estimator of the normalized covariance matrix is given by $\hat{M}_{FP}$ in (3). But, when the texture is a random variable, $\hat{M}_{FP}$ is not the ML estimator, it is an "approximate" ML estimator. The ML estimator of the normalized covariance matrix depends on the texture PDF $p_\tau(\tau)$, its expression is linked with the density generator function $h_p(x)$ by:

$$[\hat{M}_{ML}] = \frac{1}{N} \sum_{i=1}^{N} \frac{h_{p+1}\left(\mathbf{k}_i^H [\hat{M}_{ML}]^{-1} \mathbf{k}_i\right)}{h_p\left(\mathbf{k}_i^H [\hat{M}_{ML}]^{-1} \mathbf{k}_i\right)} \mathbf{k}_i \mathbf{k}_i^H, \tag{4}$$

where the expression of density generator function is given by:

$$h_p(x) = \int_0^{+\infty} \frac{1}{\tau^p} \exp\left(-\frac{x}{\tau}\right) p_\tau(\tau)\, d\tau. \tag{5}$$

2.2. Matrix log-cumulant diagram

The quantities β_1 (squared skewness) and β_2 (kurtosis) have commonly been used to characterize the distributions in the Pearson system. An alternative to the traditional β_1/β_2 parameters has been proposed by Nicolas (7): the κ_2/κ_3-plane where κ_i is the log-cumulant of order i. Fig. 1 shows a comparison between the β_1/β_2-diagram and the κ_2/κ_3-plane. Those plans are covered by a set of five distribution families issued from the Pearson system of distribution, namely Gamma (Pearson type III, in red), Inverse Gamma (Pearson type V, in blue), Fisher (Pearson type VI, in yellow), Beta (Pearson type I, in cyan) and Inverse Beta PDFs (in magenta). Note that the coordinates $(0, 3)$ in the β_1/β_2-diagram and $(0, 0)$ in the κ_2/κ_3-plane corresponds to a degenerate distribution with zero variance, equivalent to a constant value. It is represented by an orange circle. In the β_1/β_2-diagram, Beta and Inverse Beta distributions cover the same domain, whereas they are well separated in the κ_2/κ_3-plane. Moreover, for the β_1/β_2-diagram, the moments of order 4 should be computed, and for the Fisher distribution it exists only for the some specific shape parameters ($\mathcal{M} > 4$, see (20) for the meaning of $\mathcal{M}$). As the Fisher distribution has all its log-cumulant defined, the κ_2/κ_3-plane permits a whole representation of this family and has the advantage of separating between "standard" light-tailed distributions and heavy-tailed distributions.

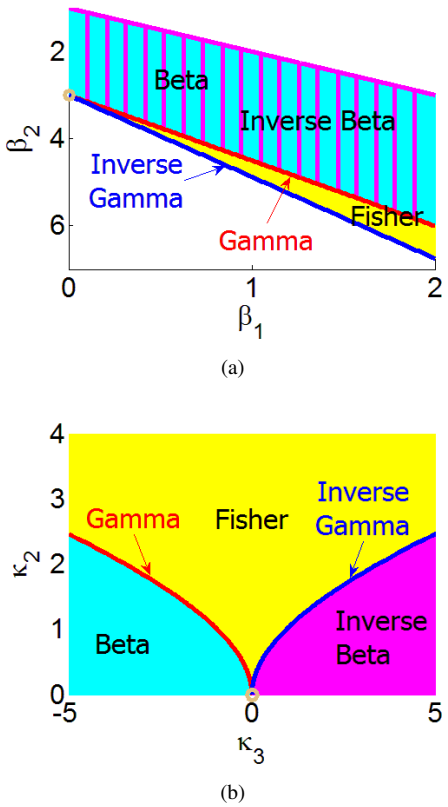

Figure 1. (a) β_1/β_2-diagram, (b) κ_2/κ_3-plane.

Recently, Anfinsen et Eltoft have proposed an extension of the κ_2/κ_3-plane based on the matrix-variate Mellin transform: the matrix log-cumulant diagram (8).

From the polarimetric product model, one can write

$[T] = \tau[M]$ where τ is the scalar texture random variable and $[M]$ is the covariance matrix of the Gaussian process, it yields that $[M]$ follows a complex Wishart distribution. Next, using matrix-variate Mellin kind statistics, they derive the expression of the ν-th order Mellin kind cumulant of $|[T]| = \tau^p |[M]|$, denoted $\kappa_\nu\{[T]\}$ as:

$$\kappa_\nu\{[T]\} = p^\nu \kappa_\nu\{\tau\} + \kappa_\nu\{[M]\}, \tag{6}$$

where:

$$\kappa_1\{[C]\} = E\Big\{ \ln |[C]| \Big\} = \int_{\Omega^+} \ln |[C]|\, p_{[C]}([C])\; d[C]$$

$$\kappa_\nu\{[C]\} = E\Big\{ \Big(\ln |[C]| - \kappa_1\{[C]\} \Big)^\nu \Big\};\;\; \nu > 1, \tag{7}$$

where Ω^+ is the cone of positive definite matrices. (6) allows separating the contribution of the texture part from the Gaussian part. After some mathematical derivation, the expression of the matrix log-cumulant is given by (8):

$$\kappa_1\{[T]\} = \psi_p^{(0)}(L) + \ln |[M]| - p\big(\ln L - \kappa_1\{\tau\} \big) \tag{8}$$

$$\kappa_\nu\{[T]\} = \psi_p^{(\nu-1)}(L) + p^\nu \kappa_\nu\{\tau\};\;\; \nu > 1, \tag{9}$$

where L is the number of looks and $\psi_p^{(\nu)}(L)$ is the ν-th order multivariate polygamma function defined by:

$$\psi_p^{(\nu)}(L) = \sum_{i=0}^{p-1} \psi^{(\nu)}(L - i), \tag{10}$$

and $\psi^{(\nu-1)}(L) = \frac{\mathrm{d}^\nu \ln \Gamma(L)}{\mathrm{d}L^\nu}$ is the ordinary polygamma function.

A representation of the matrix log-cumulant diagram (for $p = 3$ and $L = 4$) is given in Fig. 2. According to (9), for a fixed number of looks, this plan corresponds to a shifted version of the "univariate" κ_2/κ_3-plane. In the matrix log-cumulant diagram, the Wishart distribution is located by a point represented here by an orange circle. For Gamma and Inverse Gamma distributed texture, the corresponding SIRV PDFs are the classical $\mathcal{K}$ (2) and $\mathcal{G}^0$ (3) PDFs. In this plan, they are respectively represented by the red and blue curves as they are characterized by only one shape parameter. The KummerU (4), $\mathcal{W}$ and $\mathcal{M}$ PDFs are the SIRV PDFs for Fisher, Beta and Inverse Beta distributed texture. As they involve two shape parameters, those distributions are represented by a surface in the matrix log-cumulant diagram as observed in Fig. 2 (respectively in yellow, cyan and magenta).

In the next section, an overview of those multivariate PolSAR models is given for both single-look and multilook data.

3. MULTIVARIATE POLSAR MODELS

3.1. For single-look data

By using the Bayes theorem, the distribution of the target scattering vector $\mathbf{k} = \sqrt{\tau}\mathbf{z}$, denoted $p_{\mathbf{k}}(\mathbf{k})$, is obtained

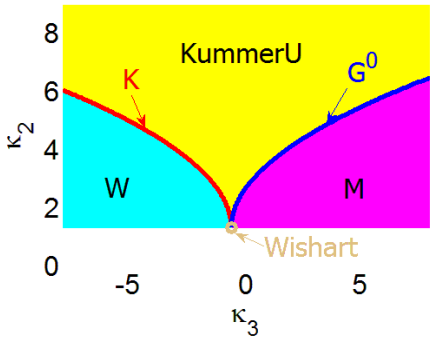

Figure 2. Matrix log-cumulant diagram.

by computing the following integral:

$$p_{\mathbf{k}}(\mathbf{k}) = \int_0^\infty p_{\mathbf{z}}(\mathbf{k}|\tau[M])\; p_\tau(\tau)\; d\tau$$
$$= \frac{1}{\pi^p |[M]|} \int_0^{+\infty} \frac{1}{\tau^p}\; \exp\Big(- \frac{\mathbf{k}^H [M]^{-1} \mathbf{k}}{\tau} \Big)\; p_\tau(\tau)\; d\tau. \tag{11}$$

To model the texture random variable, we focus here on the five distributions necessary to fully cover the matrix log-cumulant diagram, namely Gamma, Inverse Gamma, Fisher, Beta and Inverse Beta PDFs. In the following, m will refer to a scale parameter, whereas $\mathcal{L}$ and $\mathcal{M}$ will refer to shape parameters.

For each model, the texture PDF, its log-cumulant and some particular cases are first exhibit. Then, the corresponding multivariate distributions under the SIRV model are given.

Gamma distributed texture Let τ be a Gamma distributed random variable. Its PDF $p_\tau(\tau)$ is given by:

$$p_\tau(\tau) = \mathcal{G}(\tau|m, \mathcal{L}) = \frac{1}{\Gamma(\mathcal{L})} \frac{\mathcal{L}}{m} \left(\frac{\mathcal{L}\tau}{m} \right)^{\mathcal{L}-1} e^{-\frac{\mathcal{L}\tau}{m}}, \tag{12}$$

where $\mathcal{L} \geq 0$, $m > 0$ and $\tau \in \Big[0, +\infty\Big[$. A particular case of this distribution is the homothetic distribution $\mathcal{H}$ obtained when $\mathcal{L}$ tends toward infinity:

$$\lim_{\mathcal{L}\to\infty} \mathcal{G}(\tau|m, \mathcal{L}) = \mathcal{H}(\tau|m). \tag{13}$$

Its log-cumulants are given by:

$$\kappa_\nu\,(\tau) = \psi^{(\nu-1)}(\mathcal{L}), \quad \forall \nu > 1. \tag{14}$$

For a Gamma distributed texture, the PDF of the target scattering vector $\mathbf{k}$ is the $\mathcal{K}$ distribution given by (2):

$$p_{\mathbf{k}}(\mathbf{k}|[M], m, \mathcal{L}) = \frac{2}{\pi^p \Gamma(\mathcal{L}) |[M]|} \left(\frac{\mathcal{L}}{m} \right)^{\left(\frac{\mathcal{L}+p}{2}\right)}$$
$$\times \Big[\mathbf{k}^H [M]^{-1} \mathbf{k} \Big]^{\left(\frac{\mathcal{L}-p}{2}\right)} \mathrm{BesselK}_{p-\mathcal{L}} \left(2\sqrt{\frac{\mathcal{L}\, \mathbf{k}^H [M]^{-1} \mathbf{k}}{m}} \right), \tag{15}$$

where BesselK$(\cdot)$ is the modified Bessel function of the second kind.

Inverse Gamma distributed texture Let τ be an Inverse Gamma distributed random variable. Its PDF $p_\tau(\tau)$ is given by:

$$p_\tau(\tau) = \mathcal{IG}(\tau|m,\mathcal{M}) = \frac{1}{\Gamma(\mathcal{M})}\frac{1}{\mathcal{M}m}\left(\frac{\mathcal{M}m}{\tau}\right)^{\mathcal{M}+1} e^{-\frac{\mathcal{M}m}{\tau}}, \tag{16}$$

where $\mathcal{M} \geq 0$, $m > 0$ and $\tau \in \Big[0, +\infty\Big[$. The Inverse Gamma PDF tends toward the homothetic distribution for a large shape parameter:

$$\lim_{\mathcal{M}\to\infty} \mathcal{IG}(\tau|m,\mathcal{M}) = \mathcal{H}(\tau|m). \tag{17}$$

Its log-cumulants are given by:

$$\kappa_\nu(\tau) = (-1)^\nu \psi^{(\nu-1)}(\mathcal{M}), \quad \forall \nu > 1. \tag{18}$$

For an Inverse Gamma distributed texture, the target scattering vector $\mathbf{k}$ follows the $\mathcal{G}^0$ distribution given by (3):

$$p_{\mathbf{k}}(\mathbf{k}|[M],m,\mathcal{M}) = \frac{1}{\pi^p|[M]|}\frac{(\mathcal{M}m)^{\mathcal{M}}}{\Gamma(\mathcal{M})}\Gamma(p+\mathcal{M}) \times \Big(\mathbf{k}^H[M]^{-1}\mathbf{k} + \mathcal{M}m\Big)^{-(\mathcal{M}+p)}. \tag{19}$$

Fisher distributed texture Let τ be a Fisher distributed random variable. Its PDF $p_\tau(\tau)$ is given by:

$$p_\tau(\tau) = \mathcal{F}(\tau|m,\mathcal{L},\mathcal{M}) = \frac{\Gamma(\mathcal{L}+\mathcal{M})}{\Gamma(\mathcal{L})\Gamma(\mathcal{M})}\frac{\mathcal{L}}{\mathcal{M}m}\frac{\left(\frac{\mathcal{L}\tau}{\mathcal{M}m}\right)^{\mathcal{L}-1}}{\left(1+\frac{\mathcal{L}\tau}{\mathcal{M}m}\right)^{\mathcal{L}+\mathcal{M}}}, \tag{20}$$

where $\mathcal{L} \geq 0$, $\mathcal{M} \geq 0$, $m > 0$ and $\tau \in \Big[0, +\infty\Big[$. The Fisher PDF is generalization of both Gamma and Inverse Gamma PDFs as:

$$\lim_{\mathcal{L}\to\infty} \mathcal{F}(\tau|m,\mathcal{L},\mathcal{M}) = \mathcal{IG}(\tau|m,\mathcal{M}). \tag{21}$$

$$\lim_{\mathcal{M}\to\infty} \mathcal{F}(\tau|m,\mathcal{L},\mathcal{M}) = \mathcal{G}(\tau|m,\mathcal{L}). \tag{22}$$

Its log-cumulants are given by:

$$\kappa_\nu(\tau) = \psi^{(\nu-1)}(\mathcal{L}) + (-1)^\nu \psi^{(\nu-1)}(\mathcal{M}), \quad \forall \nu > 1. \tag{23}$$

For a Fisher distributed texture, the target scattering vector $\mathbf{k}$ follows the KummerU PDF given by (9):

$$p_{\mathbf{k}}(\mathbf{k}|[M],\mathcal{L},\mathcal{M},m) = \frac{1}{\pi^p|[M]|}\frac{\Gamma(\mathcal{L}+\mathcal{M})}{\Gamma(\mathcal{L})\Gamma(\mathcal{M})}\left(\frac{\mathcal{L}}{\mathcal{M}m}\right)^p \times \Gamma(p+\mathcal{M})\mathrm{U}\left(p+\mathcal{M}; 1+p-\mathcal{L}; \frac{\mathcal{L}}{\mathcal{M}m}\mathbf{k}^H[M]^{-1}\mathbf{k}\right), \tag{24}$$

where U is the confluent hypergeometric function of the second kind.

Beta distributed texture Let τ be a Beta distributed random variable. Its PDF $p_\tau(\tau)$ is given by:

$$p_\tau(\tau) = \mathcal{B}(\tau|m,\mathcal{L},\mathcal{M}) = \frac{\mathcal{L}}{\mathcal{M}m}\frac{\Gamma(\mathcal{M})}{\Gamma(\mathcal{L})\Gamma(\mathcal{M}-\mathcal{L})} \times \left(\frac{\mathcal{L}\tau}{\mathcal{M}m}\right)^{\mathcal{L}-1}\left(1-\frac{\mathcal{L}\tau}{\mathcal{M}m}\right)^{\mathcal{M}-\mathcal{L}-1}, \tag{25}$$

with $\mathcal{M} > \mathcal{L}$, $m > 0$ and $\tau \in \left[0, \frac{\mathcal{M}m}{\mathcal{L}}\right]$. This PDF has two particular cases:

$$\lim_{\mathcal{L}\to\infty} \mathcal{B}(\tau|m,\mathcal{L},\mathcal{M}) = \mathcal{H}(\tau|m). \tag{26}$$

$$\lim_{\mathcal{M}\to\infty} \mathcal{B}(\tau|m,\mathcal{L},\mathcal{M}) = \mathcal{G}(\tau|m,\mathcal{L}). \tag{27}$$

Its log-cumulants are given by:

$$\kappa_\nu(\tau) = \psi^{(\nu-1)}(\mathcal{L}) - \psi^{(\nu-1)}(\mathcal{M}), \quad \forall \nu > 1. \tag{28}$$

By using the following relation (10, Eq.13.2.6):

$$\Gamma(a)\,\mathrm{U}(a,b,z) = e^z \int_1^{+\infty} e^{-zt}(t-1)^{a-1}t^{b-a-1}dt, \tag{29}$$

with $\Re\mathrm{e}(a) > 0$ and $\Re\mathrm{e}(z) > 0$, one can proves that the expression of the target vector PDF for a Beta distributed texture is given by:

$$p_{\mathbf{k}}(\mathbf{k}|[M],m,\mathcal{L},\mathcal{M}) = \frac{1}{\pi^p|[M]|}\left(\frac{\mathcal{L}}{\mathcal{M}m}\right)^p\frac{\Gamma(\mathcal{M})}{\Gamma(\mathcal{L})} \times \exp\Big(-\frac{\mathbf{k}^H[M]^{-1}\mathbf{k}\mathcal{L}}{\mathcal{M}m}\Big) \times \mathrm{U}\left(\mathcal{M}-\mathcal{L}, -\mathcal{L}+p+1, \frac{\mathbf{k}^H[M]^{-1}\mathbf{k}\mathcal{L}}{\mathcal{M}m}\right). \tag{30}$$

Abramowitz and Stegun have shown in (10, Eq.13.1.33) that the Kummer U function can be replaced by the Whittaker W function according to the following relation:

$$\mathrm{W}_{\kappa,\mu}(z) = z^{\mu+\frac{1}{2}}\,e^{-\frac{z}{2}}\,\mathrm{U}\left(\mu-\kappa+\frac{1}{2}, 2\mu+1, z\right). \tag{31}$$

Let, $\kappa = \frac{p+\mathcal{L}+1-2\mathcal{M}}{2}$, $\mu = \frac{p-\mathcal{L}}{2}$ and $z = \frac{\mathbf{k}^H[M]^{-1}\mathbf{k}\mathcal{L}}{\mathcal{M}m}$, it yields to the $\mathcal{W}$ PDF (5) defined by:

$$p_{\mathbf{k}}(\mathbf{k}|[M],m,\mathcal{L},\mathcal{M}) = \frac{1}{\pi^p|[M]|}\left(\frac{\mathcal{L}}{\mathcal{M}m}\right)^{\frac{\mathcal{L}+p-1}{2}} \times \left(\mathbf{k}^H[M]^{-1}\mathbf{k}\right)^{\frac{\mathcal{L}-p-1}{2}}\frac{\Gamma(\mathcal{M})}{\Gamma(\mathcal{L})}\exp\left(-\frac{\mathbf{k}^H[M]^{-1}\mathbf{k}\mathcal{L}}{2\mathcal{M}m}\right) \times \mathrm{W}_{\frac{p+\mathcal{L}+1-2\mathcal{M}}{2},\frac{p-\mathcal{L}}{2}}\left(\frac{\mathbf{k}^H[M]^{-1}\mathbf{k}\mathcal{L}}{\mathcal{M}m}\right). \tag{32}$$

Inverse Beta distributed texture Let τ be an Inverse Beta distributed random variable. Its PDF $p_\tau(\tau)$ is given by:

$$p_\tau(\tau) = \mathcal{IB}(\tau|m,\mathcal{L},\mathcal{M}) = \frac{\Gamma(\mathcal{M})}{\Gamma(\mathcal{L})\Gamma(\mathcal{M}-\mathcal{L})}\left(\frac{\mathcal{M}}{\mathcal{L}m}\right) \times \left(\frac{\mathcal{M}\tau}{\mathcal{L}m}-1\right)^{\mathcal{M}-\mathcal{L}-1}\left(\frac{\mathcal{M}\tau}{\mathcal{L}m}\right)^{-\mathcal{M}}, \quad (33)$$

with $\mathcal{M} \geq \mathcal{L}$, $m > 0$ and $\tau \in \left[\frac{\mathcal{L}m}{\mathcal{M}}, +\infty\right[$. This PDF has two particular cases:

$$\lim_{\mathcal{L}\to\infty} \mathcal{IB}(\tau|m,\mathcal{L},\mathcal{M}) = \mathcal{H}(\tau|m). \quad (34)$$

$$\lim_{\mathcal{M}\to\infty} \mathcal{IB}(\tau|m,\mathcal{L},\mathcal{M}) = \mathcal{IG}(\tau|m,\mathcal{L}). \quad (35)$$

Its log-cumulants are given by:

$$\kappa_\nu(\tau) = (-1)^\nu\Big(\psi^{(\nu-1)}(\mathcal{L}) - \psi^{(\nu-1)}(\mathcal{M})\Big), \quad \forall \nu > 1. \quad (36)$$

By using the following relation (10, Eq.13.2.1):

$$\frac{\Gamma(b-a)\Gamma(a)}{\Gamma(b)}\,\mathrm{M}(a,b,z) = \int_0^1 e^{zt}t^{a-1}(1-t)^{b-a-1}dt, \quad (37)$$

with $\Re\mathrm{e}(b) > \Re\mathrm{e}(a) > 0$. $\mathrm{M}(a,b,z)$ is the confluent hypergeometric function of the first kind (KummerM), also denoted ${}_1F_1(a,b,z)$, one can proves that the expression of the target vector PDF for an Inverse Beta distributed texture is given by:

$$p_{\mathbf{k}}(\mathbf{k}|[M],m,\mathcal{L},\mathcal{M}) = \frac{1}{\pi^p|[M]|}\,\frac{\Gamma(\mathcal{M})\Gamma(p+\mathcal{L})}{\Gamma(\mathcal{L})\Gamma(p+\mathcal{M})}\left(\frac{\mathcal{M}}{\mathcal{L}m}\right)^p \times \mathrm{M}\left(p+\mathcal{L}, p+\mathcal{M}, -\frac{\mathbf{k}^H[M]^{-1}\mathbf{k}\mathcal{M}}{\mathcal{L}m}\right). \quad (38)$$

Abramowitz and Stegun have shown in (10, Eq.13.1.32) that the Kummer M function can be replaced by the Whittaker M function (denoted $\mathrm{M}_{\kappa,\mu}$) according to the following relation:

$$\mathrm{M}_{\kappa,\mu}(z) = z^{\mu+\frac{1}{2}}\,e^{-\frac{z}{2}}\,\mathrm{M}\left(\mu-\kappa+\frac{1}{2}, 2\mu+1, z\right). \quad (39)$$

Let $\kappa = \frac{\mathcal{M}-p-2\mathcal{L}}{2}$, $\mu = \frac{p+\mathcal{M}-1}{2}$ and $z = -\frac{\mathbf{k}^H[M]^{-1}\mathbf{k}\mathcal{M}}{\mathcal{L}m}$, it yields to the $\mathcal{M}$ distribution (5) defined by:

$$p_{\mathbf{k}}(\mathbf{k}|[M],m,\mathcal{L},\mathcal{M}) = \frac{1}{\pi^p|[M]|}\left(\frac{\mathcal{M}}{\mathcal{L}m}\right)^{\frac{p-\mathcal{M}}{2}}\frac{\Gamma(\mathcal{M})\Gamma(p+\mathcal{L})}{\Gamma(\mathcal{L})\Gamma(p+\mathcal{M})} \times \left(-\mathbf{k}^H[M]^{-1}\mathbf{k}\right)^{\frac{-p-\mathcal{M}}{2}}\exp\left(-\frac{\mathbf{k}^H[M]^{-1}\mathbf{k}\mathcal{M}}{2\mathcal{L}m}\right) \times \mathbf{M}_{\frac{\mathcal{M}-p-2\mathcal{L}}{2},\frac{p+\mathcal{M}-1}{2}}\left(-\frac{\mathbf{k}^H[M]^{-1}\mathbf{k}\mathcal{M}}{\mathcal{L}m}\right). \quad (40)$$

3.2. For multilook data

As for the single look case, the distributions of the covariance matrix $[T] = \tau[M]$, denoted $p_{[T]}([T])$, is obtained by using the Bayes theorem:

$$p_{[T]}([T]) = \int_0^\infty p_{[M]}([T]|\tau[M])\,p_\tau(\tau)\,d\tau = \int_0^\infty \frac{L^{Lp}|[T]|^{L-p}\exp\left\{-\frac{L}{\tau}\,\mathrm{tr}\left([M]^{-1}[T]\right)\right\}}{\pi^{\frac{p(p-1)}{2}}\Gamma(L)\cdots\Gamma(L-p+1)\tau^{Lp}|[M]|^L}\,p_\tau(\tau)\,d\tau. \quad (41)$$

For the considered texture models, the distribution of the covariance matrix are given in Table. 1.

3.3. Texture shape parameter estimators

If single look data are available, the SIRV estimation scheme introduced in Section 2 can be used to estimate the covariance matrix (3) and the texture parameter (2). Then, the texture shape parameters $\mathcal{L}$ and/or $\mathcal{M}$ can be estimated by using the maximum likelihood (9) or log-cumulants (7) methods.

Sometimes data are available only in the multilook format, *i.e.* the observed images are the non-singular covariance matrices $[T]$. In this case, the fixed point covariance matrix estimator cannot be computed and the texture shape parameters should be directly estimated from those covariance matrices. To this aim, Anfinsen et Eltoft (11) have proposed to use the second and third order matrix log-cumulants ($\kappa_2\{[T]\}$ and $\kappa_3\{[T]\}$) defined by (9). Note that those two terms are independent from the scale texture parameter m and the covariance matrix $[M]$. For KummerU, $\mathcal{W}$ and $\mathcal{M}$ distributed clutter, they depends only on the equivalent number of looks L and on the two shape parameters $\mathcal{L}$ and $\mathcal{M}$. L can be directly estimated from the covariance matrices $[T]$ according to (12). The optimal shape parameters $\hat{\mathcal{L}}$ and $\hat{\mathcal{M}}$ are estimated through a generalised least squares approach, where we minimize a criterion function representing the weighted quadratic error in the matrix log-cumulant equations. In practice, the solution is found with the nonlinear conjugate gradient method (5).

4. RESULTS

To evaluate the potential of each SIRV PDFs for the modeling of PolSAR images, three fully polarimetric C-, L- and P-band SAR images acquired by the NASA/JPL/AIRSAR sensor in 1989 over the Nezer forest, France are analyzed. Fig. 3(a) show the ground truth. A colored composition in the Pauli basis of the covariance matrices is given in Fig 3(b), 3(d) and 3(f) for the three multifrequency images. A 7×7 refined Lee filter has first been applied on each data-set to reduce the

Table 1. Covariance matrix distributions.

Texture PDF	SIRV PDF	
	Name	$p_{\mathbf{k}}(\mathbf{k})$
Homothetic	Wishart	$\frac{L^{Lp}\lvert[T]\rvert^{L-p}\exp\left\{-L\,\mathrm{tr}\left([M]^{-1}[T]\right)\right\}}{\pi^{\frac{p(p-1)}{2}}\Gamma(L)\cdots\Gamma(L-p+1)\lvert[M]\rvert^{L}}$
Gamma	$\mathcal{K}$	$\frac{2\lvert[T]\rvert^{L-p}}{\pi^{\frac{p(p-1)}{2}}\Gamma(L)\cdots\Gamma(L-p+1)\lvert[M]\rvert^{L}}\frac{1}{\Gamma(\mathcal{L})}\left(\frac{L\mathcal{L}}{m}\right)^{\frac{Lp+\mathcal{L}}{2}}\left[\mathrm{tr}\left([M]^{-1}[T]\right)\right]^{\frac{\mathcal{L}-Lp}{2}}\,\mathrm{BesselK}_{\mathcal{L}-Lp}\left(2\sqrt{\frac{L\mathcal{L}\,\mathrm{tr}\left([M]^{-1}[T]\right)}{m}}\right)$
Inverse Gamma	$\mathcal{G}^0$	$\frac{L^{Lp}\lvert[T]\rvert^{L-p}}{\pi^{\frac{p(p-1)}{2}}\Gamma(L)\cdots\Gamma(L-p+1)\lvert[M]\rvert^{L}}\frac{\Gamma(Lp+\mathcal{M})}{\Gamma(\mathcal{M})}(\mathcal{M}m)^{\mathcal{M}}\left[L\mathrm{tr}\left([M]^{-1}[T]\right)+\mathcal{M}m\right]^{-(\mathcal{M}+Lp)}$
Fisher	KummerU	$\frac{L^{Lp}\lvert[T]\rvert^{L-p}}{\pi^{\frac{p(p-1)}{2}}\Gamma(L)\cdots\Gamma(L-p+1)\lvert[M]\rvert^{L}}\frac{\Gamma(\mathcal{L}+\mathcal{M})}{\Gamma(\mathcal{L})\Gamma(\mathcal{M})}\left(\frac{\mathcal{L}}{\mathcal{M}m}\right)^{Lp}\Gamma\left(Lp+\mathcal{M}\right)U\left(Lp+\mathcal{M},1+Lp-\mathcal{L},\frac{L\,\mathrm{tr}\left([M]^{-1}[T]\right)\mathcal{L}}{\mathcal{M}m}\right)$
Beta	$\mathcal{W}$	$\frac{\lvert[T]\rvert^{L-p}}{\pi^{\frac{p(p-1)}{2}}\Gamma(L)\cdots\Gamma(L-p+1)\lvert[M]\rvert^{L}}\left(\frac{L\mathcal{L}}{\mathcal{M}m}\right)^{\frac{\mathcal{L}+Lp-1}{2}}\left[\mathrm{tr}\left([M]^{-1}[T]\right)\right]^{\frac{\mathcal{L}-Lp-1}{2}}\frac{\Gamma(\mathcal{M})}{\Gamma(\mathcal{L})}\exp\left\{-\frac{L\mathcal{L}}{2\mathcal{M}m}\,\mathrm{tr}\left([M]^{-1}[T]\right)\right\}$ $\times_{\mathrm{W}}\frac{Lp+\mathcal{L}+1-2\mathcal{M}}{2},\frac{Lp-\mathcal{L}}{2}\left(\frac{L\mathcal{L}}{\mathcal{M}m}\,\mathrm{tr}\left([M]^{-1}[T]\right)\right)$
Inverse Beta	$\mathcal{M}$	$\frac{\lvert[T]\rvert^{L-p}}{\pi^{\frac{p(p-1)}{2}}\Gamma(L)\cdots\Gamma(L-p+1)\lvert[M]\rvert^{L}}\left(\frac{L\mathcal{M}}{\mathcal{L}m}\right)^{\frac{Lp-\mathcal{M}}{2}}\left[-\mathrm{tr}\left([M]^{-1}[T]\right)\right]^{\frac{-Lp-\mathcal{M}}{2}}\frac{\Gamma(\mathcal{M})\Gamma(Lp+\mathcal{L})}{\Gamma(\mathcal{L})\Gamma(Lp+\mathcal{M})}\exp\left\{-\frac{L\mathcal{M}}{2\mathcal{L}m}\,\mathrm{tr}\left([M]^{-1}[T]\right)\right\}$ $\times_{\mathrm{M}}\frac{\mathcal{M}-Lp-2\mathcal{L}}{2},\frac{Lp+\mathcal{M}-1}{2}\left(-\frac{L\mathcal{M}}{\mathcal{L}m}\,\mathrm{tr}\left([M]^{-1}[T]\right)\right)$

speckle (13). Four classes of 400 pixels have then been extracted from each data-set, *i.e.* bare soil (yellow), 8-11 years (blue), 15-19 years (red) and 33-41 years (green). In order to visualise the statistical variation of the log-cumulants, multiple log-cumulant estimates have been obtained by bootstrap sampling. Here, 200 samples have been considered to estimate one log-cumulant realization. Fig. 3(c), 3(e) and 3(g) show the texture log-cumulant diagrams for the Nezer forest image at C-, L- and P-band. The yellow, blue, red and green points correspond to the estimated log-cumulants for the four considered classes. Note that here we have removed the speckle part of the MLCs. Thus, the texture log-cumulant diagrams are centered in (0,0), which is the case of no texture. Those texture log-cumulant diagrams motivate the use of the $\mathcal{W}$ and $\mathcal{M}$ distributions for the statistical modeling of PolSAR images.

5. CONCLUSION AND PERSPECTIVES

In this paper two new families of Probability Density Functions (PDFs) for the polarimetric target vector and the polarimetric covariance matrix have been introduced, namely the $\mathcal{W}$ and $\mathcal{M}$ distributions. These families complete the diagram spanned by the second and third-order matrix log-cumulants, and contribute to a holistic theory for statistical modeling of PolSAR data based on the doubly stochastic product model with a scalar texture variable.

Further works will deal with the use of those multivariate models in many applications such as segmentation, classification and change detection.

ACKNOWLEDGMENT

The authors would like to thank NASA/JPL and Laurent Ferro-Famil for providing the AIRSAR images over the Nezer forest.

REFERENCES

[1] J.S. Lee, M.R. Grunes, T.L. Ainsworth, L.J. Du, D.L. Schuler, and S.R. Cloude, "Unsupervised Classification Using Polarimetric Decomposition and the Complex Wishart Classifier," *IEEE Transactions on Geoscience and Remote Sensing*, vol. 37, no. 5, pp. 2249–2258, 1999.

[2] J.S. Lee, D.L. Schuler, R.H. Lang, and K.J. Ranson, "K-Distribution for Multi-Look Processed Polarimetric SAR Imagery," in *Geoscience and Remote Sensing, IGARSS '94, Pasadena, California, United States*, 1994, pp. 2179–2181.

[3] C.C. Freitas, A.C. Frery, and A.H. Correia, "The Polarimetric G Distribution for SAR Data Analysis," *Environmetrics*, vol. 16, pp. 13–31, 2005.

[4] L. Bombrun and J.-M. Beaulieu, "Fisher Distribution for Texture Modeling of Polarimetric SAR Data," *IEEE Geoscience and Remote Sensing Letters*, vol. 5, no. 3, pp. 512–516, July 2008.

[5] S.N. Anfinsen, *Application of the Matrix-Variate Mellin Transform to Analysis of Polarimetric Synthetic Aperture Radar Data*, Ph.D. thesis, University of Tromsø, Tromsø, Norway, 2010.

[6] F. Pascal, Y. Chitour, J. P. Ovarlez, P. Forster, and P. Larzabal, "Covariance Structure Maximum-Likelihood Estimates in Compound Gaussian Noise: Existence and Algorithm Analysis," *IEEE*

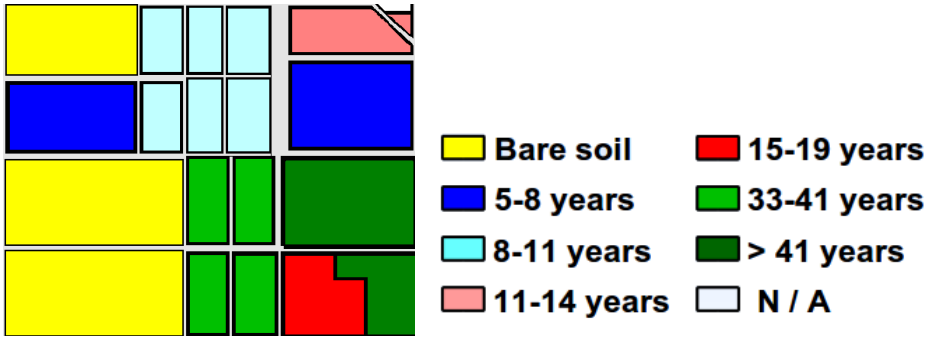

(a) ground truth

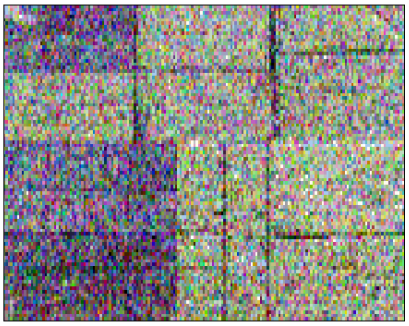

(b) C-band Pauli RGB image

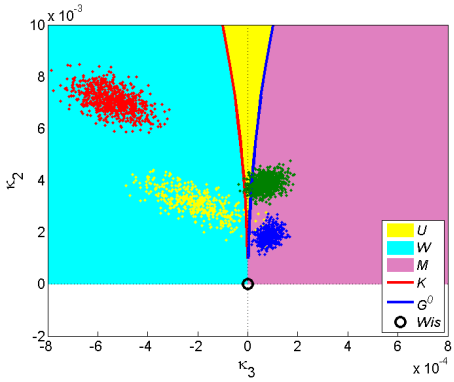

(c) C-band texture log-cumulant diagram

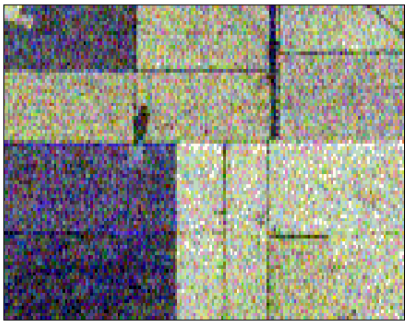

(d) L-band Pauli RGB image

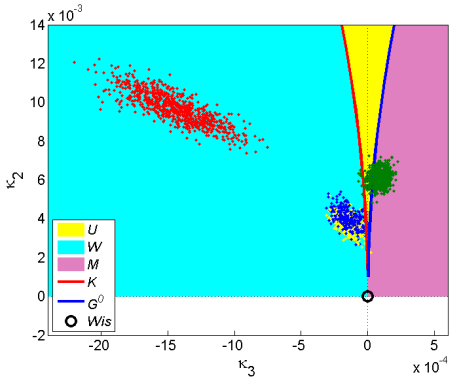

(e) L-band texture log-cumulant diagram

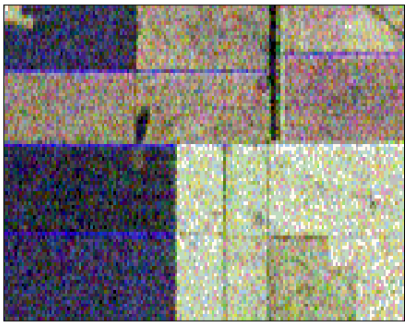

(f) P-band Pauli RGB image

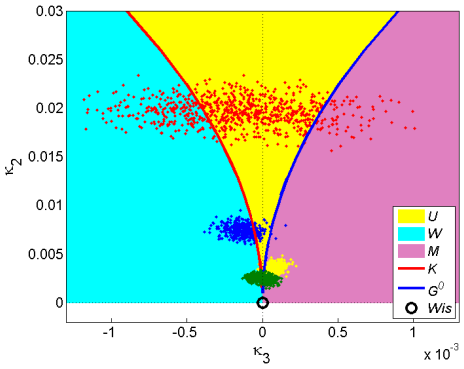

(g) P-band texture log-cumulant diagram

Figure 3. Texture log-cumulant diagrams at C-, L- and P-band for the PolSAR images acquired by the NASA/JPL/AIRSAR sensor over the Nezer forest, France.

Transactions on Signal Processing, vol. 56, no. 1, pp. 34–48, 2008.

[7] J-M. Nicolas, "Application de la Transformée de Mellin: Étude des Lois Statistiques de l'Imagerie Cohérente," in *Rapport de recherche, 2006D010*, 2006.

[8] S.N. Anfinsen and T. Eltoft, "Analysis of Multilook Polarimetric Radar Data with the Matrix-Variate Mellin Transform," in *EUSAR, Aachen, Germany*, 2010, pp. 485–488.

[9] L. Bombrun, G. Vasile, M. Gay, and F. Totir, "Hierarchical Segmentation of Polarimetric SAR Images using Heterogeneous Clutter Models," *IEEE Transactions on Geoscience and Remote Sensing, to appear*, 2011.

[10] M. Abramowitz and I.A. Stegun, *Handbook of Mathematical Functions With Formulas, Graphs, and Mathematical Tables*, 1964.

[11] S. N. Anfinsen and T. Eltoft, "Application of the Matrix-variate Mellin Transform to Analysis of Polarimetric Radar Images," *IEEE Transactions on Geoscience and Remote Sensing, to appear*, 2011.

[12] S. N. Anfinsen, A. P. Doulgeris, and T. Eltoft, "Estimation of the Equivalent Number of Looks in Polarimetric Synthetic Aperture Radar Imagery," *IEEE Transactions on Geoscience and Remote Sensing*, vol. 47, no. 11, pp. 3795–3809, November 2009.

[13] J.S. Lee, "Refined filtering of image noise using local statistics," *Computer graphics and image processing*, vol. 15, no. 4, pp. 380–389, 1981.